Chem

CellPress

Article

Cobalt-Catalyzed Asymmetric Synthesis of *gem*-Bis(silyl)alkanes by Double Hydrosilylation of Aliphatic Terminal Alkynes

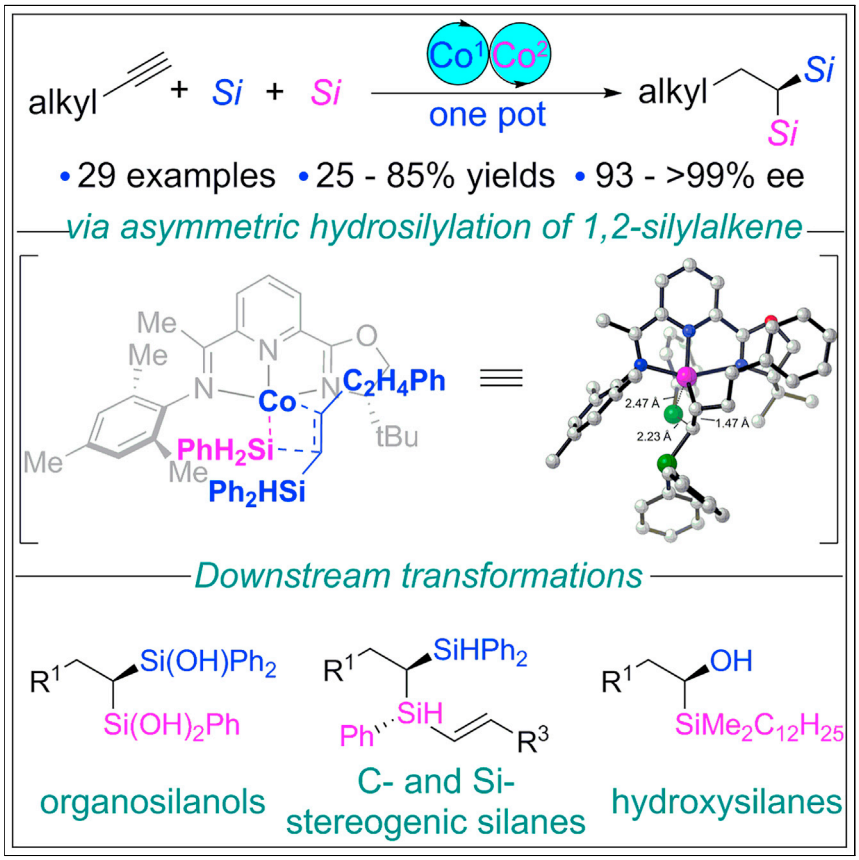

A cobalt-catalyzed sequential highly enantioselective double hydrosilylation of aliphatic alkynes for the precise synthesis of chiral *gem*-bis(silyl)alkanes was achieved. This protocol used relatively simple and available starting materials to construct more valuable products with excellent chemo-, regio- and enantioselectivities. Synthetic versatility of *gem*-bis(silyl)alkanes was demonstrated by the synthesis of chiral organosilanols and α-hydroxysilanes and hydrosilylation of alkynes to construct chiral silanes. The control experiments, isotopic labeling experiments, kinetic studies, and density functional theory calculations were conducted to elucidate the reaction mechanism.

Jun Guo, Hongliang Wang, Shipei Xing, Xin Hong, Zhan Lu

hxchem@zju.edu.cn (X.H.)
luzhan@zju.edu.cn (Z.L.)

HIGHLIGHTS

Precise synthesis of chiral *gem*-bis(silyl)alkanes with dihydro- and trihydrosilane

Dual cobalt catalysis for sequential double hydrosilylation of alkynes

Readily available starting materials under mild reaction conditions

The proposed mechanism is supported by kinetic studies and DFT calculations

Guo et al., Chem 5, 1–15
April 11, 2019 © 2019 Elsevier Inc.
https://doi.org/10.1016/j.chempr.2019.02.001

Please cite this article in press as: Guo et al., Cobalt-Catalyzed Asymmetric Synthesis of *gem*-Bis(silyl)alkanes by Double Hydrosilylation of Aliphatic Terminal Alkynes, Chem (2019), https://doi.org/10.1016/j.chempr.2019.02.001

Chem

CellPress

Article

Cobalt-Catalyzed Asymmetric Synthesis of *gem*-Bis(silyl)alkanes by Double Hydrosilylation of Aliphatic Terminal Alkynes

Jun Guo,[1,2] Hongliang Wang,[1,2] Shipei Xing,[1] Xin Hong,[1,*] and Zhan Lu[1,3,*]

SUMMARY

Chiral organosilanes are of great value in asymmetric synthesis, functional materials, and medicinal chemistry. Compared with single-silyl compounds, bis(silyl) ones are understudied because of the lack of the efficient synthetic protocols. The development of efficient synthetic approaches to access bis(silyl) compounds is highly desirable for studying their basic properties and potential utilities. Here, a cobalt-catalyzed sequential double hydrosilylation of aliphatic alkynes was developed to synthesize highly enantioenriched *gem*-bis(silyl)alkanes. This protocol used simple aliphatic alkynes and silanes to construct valuable chiral *gem*-bis(silyl)alkanes. The control experiments, isotopic labeling experiments, kinetic studies, and density functional theory calculations were conducted to elucidate the reaction mechanism. The synthetic versatility of *gem*-bis(silyl)alkanes was demonstrated by the synthesis of chiral organosilanols, α-hydroxysilanes through selective C–Si bond transformation and hydrosilylation of alkynes to construct chiral silanes containing adjacent C-stereocenter and Si-stereocenter.

INTRODUCTION

Chiral organosilanes are of great value in asymmetric synthesis[1–6] and functional materials.[7–9] Furthermore, many organosilicon compounds are bioactive and can be employed as silicon-containing drugs.[10–12] To date, several protocols have been developed to efficiently synthesize chiral organosilanes with carbon-stereogenic centers or silicon-stereogenic centers, such as asymmetric hydrosilylation of unsaturated bonds,[13–24] desymmetrization of prochiral silanes,[25–31] and asymmetric silicon-hydrogen bond insertions.[32–34] Compared with single-silyl compounds, bis(silyl) ones are understudied because of the lack of efficient synthetic protocols.[35–38] The development of efficient synthetic processes to access various bis(silyl) compounds is highly desirable for studying their basic properties and exploring their potential utilities.

Although sequential double hydrosilylation of alkynes enabled by hydrosilylation of alkenyl silanes as the key step was considered one of the most ideal methods for synthesizing bis(silyl) compounds because of the challenge of controlling the chemo-, regio-, and enantioselectivities from multicomponents, double hydrosilylations of alkynes have been rare. In 2002, Hayashi reported a successive platinum and palladium-cocatalyzed double 1,2-hydrosilylation of arylacetylenes for the synthesis of 1,2-diols with excellent enantioselectivity; however, the reaction of aliphatic alkynes has not been reported[15] (Scheme 1A). Therefore, the development of highly enantioselective double hydrosilylation of aliphatic alkynes is highly desirable.

The Bigger Picture

Chiral organosilanes are important synthetic intermediates for chiral catalysts, functional materials, and silasubstitution in medicinal chemistry. Because of the absence of highly efficient catalytic synthetic methods, enantiopure polysilyl-substituted compounds are rare and their applications are not well explored. Our methodology enables double hydrosilylation of aliphatic alkynes for the construction of unique chiral *gem*-bis(silyl)alkanes via cobalt catalysis with excellent chemo-, regio-, and enantioselectivity. We anticipate that this strategy will be a useful tool for synthesis of diverse chiral organosilanes. Furthermore, we also expect the unique *gem*-bis(silyl)alkanes will be employed not only in stereoselective organic synthesis but also in chiral catalyst and functional materials.

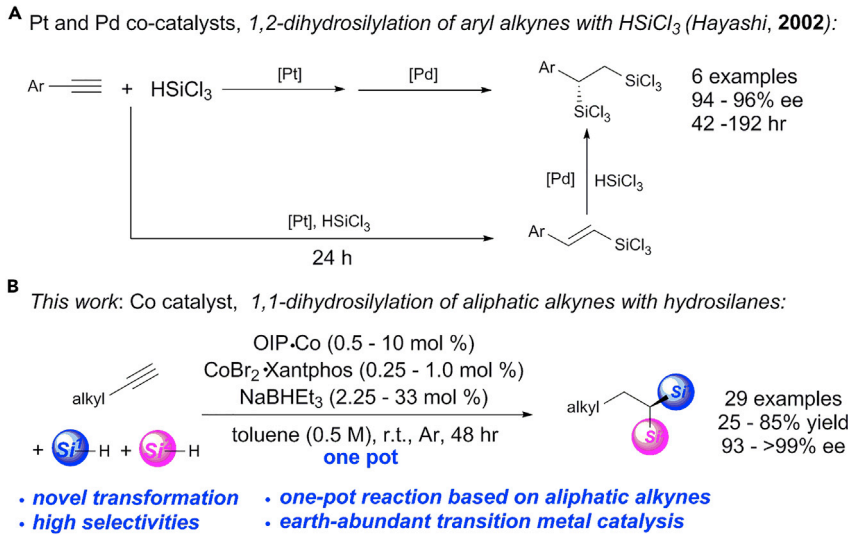

Scheme 1. Asymmetric Double Hydrosilylation of Alkynes

Because of the low cost, abundance, and low toxicity of cobalt, as well as good functional-group tolerance, cobalt-catalyzed transformation[39–55] has emerged as a hot topic in organic chemistry. In 2017, our group reported an example on $CoBr_2$•Xantphos-catalyzed *anti*-Markovnikov hydrosilylation of phenylacetylene to afford (*E*)-alkenyl silane.[20] Most recently, during the preparation of our paper, the Ge group described a cobalt-catalyzed (*E*)-selective *anti*-Markovnikov hydrosilylation of terminal alkynes.[56] Inspired by the previous works on cobalt-catalyzed hydrosilylation of alkynes and enantioselective hydrosilylation of unsaturated bonds,[20–22,24] here, we developed a highly enantioselective synthesis of *gem*-bis(silyl)alkanes enabled by $CoBr_2$•Xantphos- and $CoBr_2$•OIP (OIP = oxazoline-imino-pyridine)-catalyzed sequential asymmetric double 1,1-hydrosilylation of aliphatic alkynes by using a combination of dihydrosilanes and trihydrosilanes as the silyl source (Scheme 1B). To realize the above transformation, there lie several challenges: (1) how to control the reactivity of two different silanes in which dihydrosilanes have a similar silicon-hydrogen bond dissociation free energy with trihydrosilanes,[57] (2) how to control the complicated regioselectivities in the sequential reaction (1,1- versus 1,2- versus 2,1- versus 2,2-bis(silyl)alkanes),[58] and (3) how to achieve the high enantioselectivity in hydrosilylation of 1,2-disubstituted aliphatic alkenes.

RESULTS AND DISCUSSION

Initially, we chose but-3-yn-1-ylbenzene **1a** as a simple model substrate, diphenylsilane and phenylsilane as two different silanes. The reaction of **1a** with Ph_2SiH_2 and $PhSiH_3$ in the presence of 1.0 mol % of $CoBr_2$•Xantphos, 5.0 mol % of cobalt precatalyst **L1**•$CoCl_2$, and 18 mol % of $NaBHEt_3$ in a solution of toluene (0.5 M) at room temperature for 24 h was carried out to afford the designed product **2a** (Figures S11 and S92) in 82% yield but with only 9.1% ee and without 1,2-dihydrosilylation isomer (entry 1, Table 1). With the increased steric hindrance of the group on oxazoline (Bn, *i*Pr, and *t*Bu), yields of **2a** were decreased from 74% to 27%; however, enantioselectivities were sharply increased from 43.0% to 99.9% (entries 2–4). When 2,4,6-trimethyl-aniline-derived ligand **L5** (Figure S10) was used, the yield of **2a** increased slightly (entry 5). When the more hindered 2,6-diisopropyl-aniline-derived ligand **L6** was used, the only product of single hydrosilylation with Ph_2SiH_2 alkenyl

[1]Department of Chemistry, Zhejiang University, Hangzhou, Zhejiang 310058, China

[2]These authors contributed equally

[3]Lead Contact

*Correspondence: hxchem@zju.edu.cn (X.H.), luzhan@zju.edu.cn (Z.L.)

https://doi.org/10.1016/j.chempr.2019.02.001

Please cite this article in press as: Guo et al., Cobalt-Catalyzed Asymmetric Synthesis of *gem*-Bis(silyl)alkanes by Double Hydrosilylation of Aliphatic Terminal Alkynes, Chem (2019), https://doi.org/10.1016/j.chempr.2019.02.001

Table 1. Optimizations

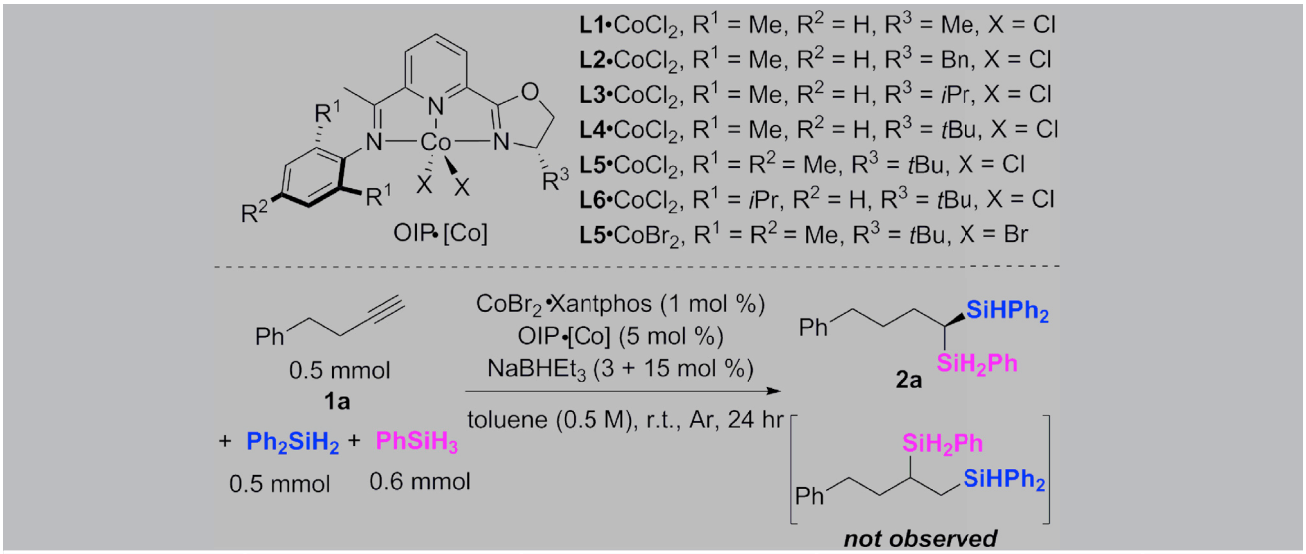

Entry	[Co]	Solvent	Yield of 2a (%)[a]	ee of 2a (%)[b]
1	L1•$CoCl_2$	toluene	82	9.1
2	L2•$CoCl_2$	toluene	74	43.0
3	L3•$CoCl_2$	toluene	72	80.3
4	L4•$CoCl_2$	toluene	27	99.9
5	L5•$CoCl_2$	toluene	32	99.9
6	L6•$CoCl_2$	toluene	<3	~
7	L5•$CoBr_2$	toluene	46	99.9
8	L5•$CoBr_2$	Et_2O	17	99.9
9	L5•$CoBr_2$	THF	10	~
10	L5•$CoBr_2$	1,4-dioxane	33	99.9
11	L5•$CoBr_2$	*n*-hexane	26	99.9
12[c]	L5•$CoBr_2$	toluene	72	99.9
13[c,d]	L5•$CoBr_2$	toluene	84[e]	99.9
14[d,f]	L5•$CoBr_2$	toluene	<1	~

[a]Yields were determined by ^{1}H NMR with TMSPh as an internal standard.
[b]ee values were determined by chiral HPLC.
[c]$CoBr_2$•Xantphos (1 mol %) and L5•$CoBr_2$ (10 mol %).
[d]48 h.
[e]Isolated yield.
[f]Without $NaBHEt_3$.

silane **3a** was observed in 94% yield (entry 6). The yield of **2a** was increased to 46% when cobalt bromide complex was used instead of cobalt chloride complex (entry 7). After screening a series of solvents, no better results were obtained (entries 8–11). After the catalyst loading was increased to 10 mol %, the yield of **2a** was increased to 72% (entry 12). The reaction for 48 h afforded **2a** in 84% isolated yield (entry 13). The control reaction without $NaBHEt_3$ was also conducted to afford **3a** and an intermediate of alkyne hydrosilylation with $PhSiH_3$ **3b** in 10% and 22% yield, respectively. However, no designed product was observed (entry 14). The standard conditions are identified as 0.5 mmol of alkyne, 0.5 mmol of Ph_2SiH_2, 0.6 mmol of $PhSiH_3$, 1 mol % of $CoBr_2$•Xantphos, 10 mol % of L5•$CoBr_2$ (see Data S1), and 33 mol % of $NaBHEt_3$ in 1.0 mL of toluene for 48 h.

Please cite this article in press as: Guo et al., Cobalt-Catalyzed Asymmetric Synthesis of *gem*-Bis(silyl)alkanes by Double Hydrosilylation of Aliphatic Terminal Alkynes, Chem (2019), https://doi.org/10.1016/j.chempr.2019.02.001

substrate scope for silanes:

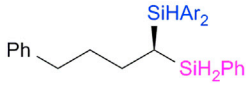

2b, Ar = 4-*t*BuC$_6$H$_4$, 85% yield, 99% ee
2c, Ar = 4-ClC$_6$H$_4$, 72% yield, 98% ee
2d, Ar = 3,5-*di*MeC$_6$H$_3$, 82% yield, >99% ee
2e, Ar = 2-naphthyl, 83% yield, 99% ee

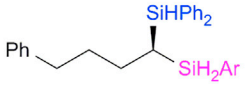

2f, Ar = 4-OMeC$_6$H$_4$, 68% yield, >99% ee
2g, Ar = 4-ClC$_6$H$_4$, 51% yield, >99% ee

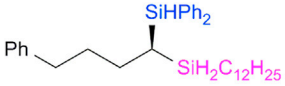

2h, 78% yield, 98% ee

substrate scope for alkynes:

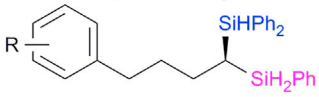

2i, R = 4-Ph, 76% yield, >99% ee
2j, R = 4-CF3, 61% yield, 98% ee
2k, R = 4-Me, 52%yield, 98% ee
2l, R = 3-Me, 68% yield, >99% ee
2m, R = 2-Me, 41% yield, 99% ee
2n, R = 3,5-*di*Me, 55% yield, 98% ee
2o, R = 1-naphthyl, 73% yield, 99% ee

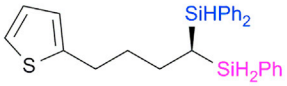

2p, 58% yield, 99% ee

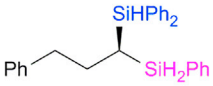

2q, 82% yield, 96% ee

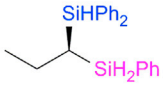

2r, 50% yield, 96% ee

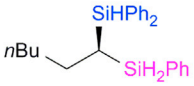

2s, 59% yield, >99% ee

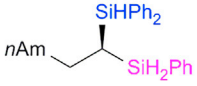

2t, 75% yield, 99% ee

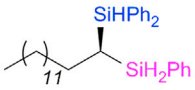

2u, 64% yield, 99% ee

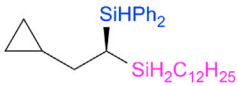

2v[b], 56% yield, >99% ee

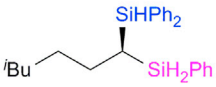

2w, 82% yield, 99% ee

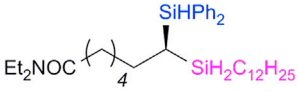

2x[b], 25% yield, 98% ee

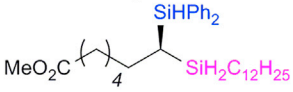

2y[b], 32% yield, 98% ee

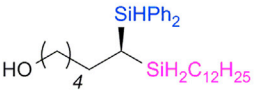

2z[b], 61% yield, 98% ee

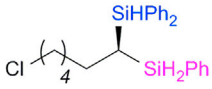

2aa, 71% yield, 99% ee

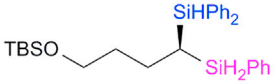

2ab, 84% yield, >99% ee

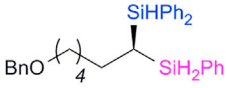

2ac, 57% yield, >99% ee

Scheme 2. Scope of Chiral Bis(silyl)alkanes

[a]Alkynes (0.5 mmol), Ph_2SiH_2 (0.5 mmol), $PhSiH_3$ (0.5 mmol), $CoBr_2$•Xantphos (1mol %), and **L5**•$CoBr_2$ (10 mol %), 48 h.
[b]**L$_3$**•$CoBr_2$ instead of **L5**•$CoBr_2$.

With the optimal reaction conditions in hand, the substrate scope was illustrated in Scheme 2. First, the scope of silanes was investigated. Various dihydrosilanes or trihydrosilanes containing electron-donating or withdrawing groups on the phenyl ring were investigated to afford the corresponding chiral *gem*-bis(silyl)alkanes **2b–2g** (Figures S13–S23 and S93–S98) in 51%–85% yield with 98% to >99% ee. Interestingly, alkyl silane could also be transformed to chiral silane **2h** (Figures S24–S26 and S99) in 78% yield with 98% ee. As far as we know, it is the first time that highly enantioselective hydrosilylation has been achieved with alkyl trihydrosilane.

Please cite this article in press as: Guo et al., Cobalt-Catalyzed Asymmetric Synthesis of *gem*-Bis(silyl)alkanes by Double Hydrosilylation of Aliphatic Terminal Alkynes, Chem (2019), https://doi.org/10.1016/j.chempr.2019.02.001

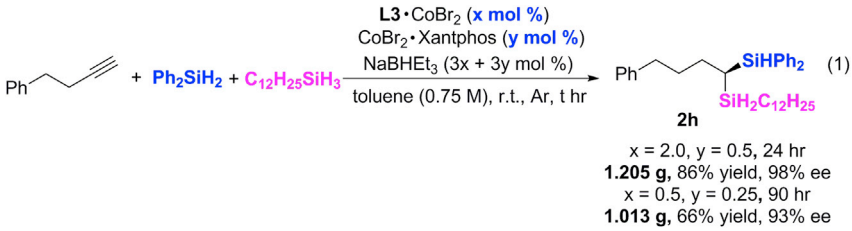

Scheme 3. Gram-Scale Reactions

Next, the scope of aliphatic alkynes was also examined. The reactions of substrates bearing withdrawing substituents **1i** and **1j** could afford **2i** (Figures S26–S27 and S100) and **2j** (Figures S28–S30 and S101) in 76% yield with >99% ee and 61% yield with 98% ee, respectively. When substrates contained *para*-, *meta*-, or *ortho*-methyl substituents on the phenyl ring, all of them could be delivered to the corresponding products **2k–2n** (Figures S31–S38 and S102–S105) in 41%–68% yields with 98% to >99% ee. The polycycle 1-naphthyl (**1o**) and heterocycle 2-thienyl (**1p**) could be tolerated well to afford **2o** (Figures S39, S40, and S106) and **2p** (Figures S41, S42, and S107) in 73% and 58% yield with 99% ee, respectively. Prop-2-yn-1-ylbenzene (**1q**) reacted smoothly to afford **2q** (Figures S43, S44, and S108) in 82% yield and 96% ee. The influence of different carbon chain length of aliphatic alkynes was studied to afford **2r–2u** (Figures S45–S52 and S109–S112) and **2w** (Figures S55, S56, and S114) in 50%–82% yields with 96% to >99% ee. The reaction of substrate bearing cyclopropyl **1v** was carried out to give **2v** (Figures S53, S54, and S113) in 56% yield and >99% ee with $C_{12}H_{25}SiH_3$ instead of $PhSiH_3$ and with more reactive and less hindered ligand **L3** instead of **L5**. The reason for choosing $C_{12}H_{25}SiH_3$ as a trihydrosilane was that, for some substrates, alkyl trihydrosilane was more reactive than the aryl one under these catalytic conditions. Substrates bearing various functional groups, such as amide (**1x**), ester (**1y**), free alcohol (**1z**), halide (**1aa**), and ethers (**1ab** and **1ac**), were also suitable to yield the corresponding chiral silanes **2x–2ac** (Figures S57–S67 and S115–S120) in 25%–84% yields with 98% to >99% ee. There are six examples of which the yields are around or below 50% (three examples for yield below 50% and three examples for yield around 50%). For these cases, there are actually around 20% of hydrogenation byproducts of alkenyl silanes in this transformation (density functional theory [DFT] calculation; see Figures S7 and S9). It had been reported that the cobalt complex could also promote both hydrogenation and hydrosilylation reaction of alkene with silanes.[59] It might be the reason why, in these cases, isolated yields of products are around or below 50%. When phenylacetylene was used, only alkyne hydrosilylation product with Ph_2SiH_2, i.e., (*E*)-alkenyl silane, was obtained in 97% yield. We also tried to employ this catalytic system to the general internal alkenes. Unfortunately, when pent-3-en-1-ylbenzene was subjected to this system, no reaction occurred (for details, see Figures S6 and S8 and Scheme S1). The absolute configuration was verified by X-ray diffraction of the corresponding dihydroxyl silanol **5e** (Figure S20; Data S2) of product **2e**, and the other products were then assigned by analogy.

To demonstrate the synthetic utility, we conducted gram-scale reactions smoothly by using 0.5 mol % of $CoBr_2$•Xantphos with 2.0 mol % of L_3•$CoBr_2$ for 24 h or 0.25 mol % of $CoBr_2$•Xantphos with 0.5 mol % of L_3•$CoBr_2$ for 90 h to afford **2h** in 86% yield with 98% ee or 66% yield with 93% ee, respectively (Scheme 3, equation 1). Additionally, the piperidine derivative **1ad** and desloratadine derivative **1ae** could also be transformed smoothly under standard conditions to **2ad** (Figure S68) and **2ae** (Figure S69) in 65% and 75% yields, respectively (see Supplemental Information).

Please cite this article in press as: Guo et al., Cobalt-Catalyzed Asymmetric Synthesis of *gem*-Bis(silyl)alkanes by Double Hydrosilylation of Aliphatic Terminal Alkynes, Chem (2019), https://doi.org/10.1016/j.chempr.2019.02.001

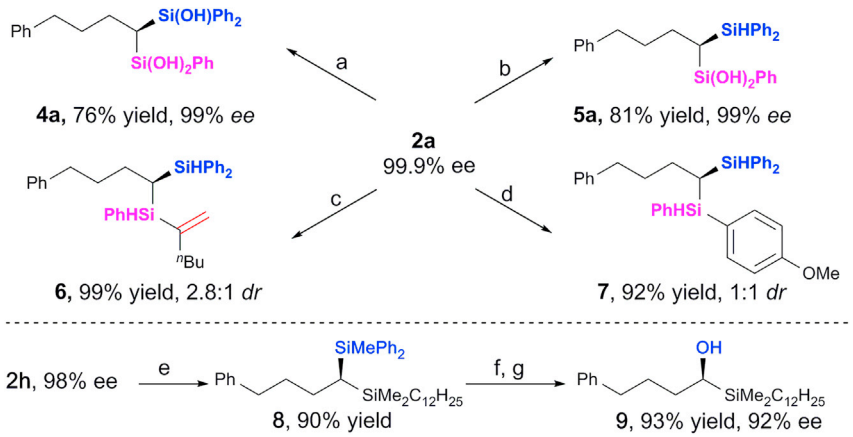

Scheme 4. Derivatizations

Reaction conditions: (a) catalytic Pd/C (20 wt %), Et_2O/H_2O = 10/1, v/v, room temperature (RT), overnight; (b) $KHCO_3$ (0.5 equiv), H_2O_2 (30% aq., 2.0 equiv), MeOH/THF = 1/1, v/v, RT, 5 min; (c) $[Ru(\eta^5\text{-Cp*})(CH_3CN)_3]Cl_2$ (4 mol %), DCM, 20°C, 40 h; (d) LiCl (5.0 equiv), 4-$OMeC_6H_4MgBr$ (5.0 equiv), THF, 80°C, 41 h; (e) CH_2I_2 (50 equiv), $ZnEt_2$ (30 equiv), 1,2-dichloroethane, RT, 40 h; (f) BF_3.2AcOH (10 equiv), $CHCl_3$, 65°C, 16 h; (g) KF (4.0 equiv), $KHCO_3$ (4.0 equiv), H_2O_2 (30% aq., 23 equiv), MeOH/THF = 1/1, v/v, 65°C, 12 h.

Organosilanols have important applications in various fields,[60] such as in polymetric materials science, organic synthesis, and medicinal chemistry. The chiral bis(silyl) alkane **2a** could be completely oxidized to chiral silanols **4a**[61] (Figures S12 and S122) or selectively oxidized to **5a**[62] (Figures S70 and S121) in 76% or 81% yield, respectively (Scheme 4). The **2a** could also undergo ruthenium-catalyzed hydrosilylation of alkyne to afford vinyl silane **6** (Figure S71) in 99% yield with a diastereomeric ratio (d.r.) of 2.8:1.[63] The reaction of **2a** with Grignard reagent gave **7** (Figure S72) in 92% yield with a d.r. of 1:1.[64] Interestingly, after being methylated,[24] product **2h** could undergo Fleming-Tamao oxidation[65] to afford chiral α-hydroxysilanes (**9**)[66] (Figures S74 and S123), which have been utilized for stereocontrolled C–C bond formation.

Because of their unique properties, chiral organosilanes containing a Si-stereocenter have attracted increasing attention in medicinal chemistry and material sciences.[24,67] However, the synthesis of Si-stereogenic silanes is undoubtedly one of the most challenging aspects of organosilicon chemistry.[68] Here, using the obtained chiral silanes **2**, a $CoBr_2$•Xantphos-catalyzed hydrosilylation of alkynes to construct chiral silanes containing adjacent C-stereocenter and Si-stereocenter (**10**) was presented (Scheme 5). A variety of substrates containing functional groups, such as halogen, ether, ester, amide, alkene, and free alcohol, were tolerated well to afford the corresponding products **10a–10l** (Figures S75–S86) in 84%–96% yields.

Several control experiments were conducted to elucidate the possible reaction pathway (Scheme 6). The competitive reaction of **1a** with Ph_2SiH_2 and $PhSiH_3$ using 1 mol % of $CoBr_2$•Xantphos as precatalyst and 3 mol % of $NaBHEt_3$ as reductant in toluene (0.5 M) for 5 min was carried out to give (*E*)-β-alkenyl silane **3a** in 93% yield and (*E*)-β-alkenyl phenyl silane **3b** in trace yield (equation 2, Scheme 6).[69] **3a** could react with $PhSiH_3$ smoothly to afford **2a** in 74% yield with >99% ee under standard conditions without $CoBr_2$•Xantphos; however, only hydrogenation product **11** was obtained when **3b** reacted with Ph_2SiH_2. These two experiments indicated that **3a** might be the reaction intermediate (equations 3 and 4, Scheme 6). Two control

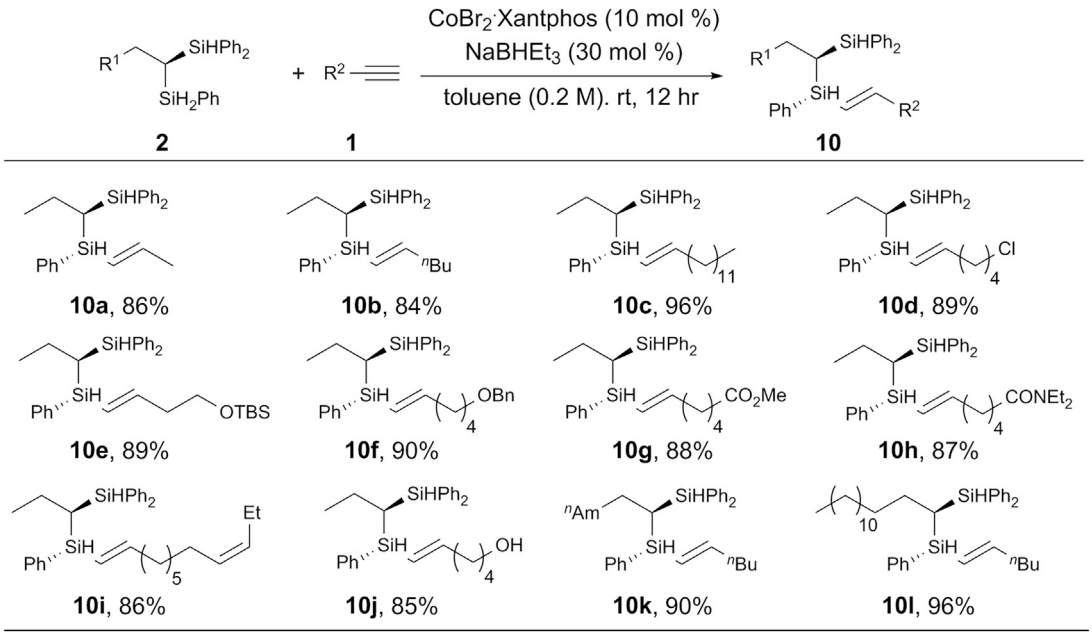

Scheme 5. Synthesis of Chiral Silanes Containing Adjacent C- and Si-Stereocenters
The diastereomeric excess of all the substrates is about 11:1.

experiments omitting $CoBr_2$•Xantphos or **L5**•$CoBr_2$ were conducted: without $CoBr_2$•Xantphos, a mixture of product **2a** (12% yield), **11** (18% yield), **3a** (12% yield), and α-alkenyl silane **12** (30% yield) was observed (equation 5, Scheme 6); without **L5**•$CoBr_2$, **2a** and **3a** were obtained in 13% and 70% yield, respectively (equation 6, Scheme 6). Equations 5 and 6 underscore the challenges in achieving the high regio- and enantioselectivities observed in our catalytic system. These control experiments indicated that the reaction might mainly undergo $CoBr_2$•Xantphos-catalyzed hydrosilylation of aliphatic alkynes with dihydrosilanes followed by OIP•$CoBr_2$-catalyzed asymmetric hydrosilylation of alkenyl silanes with the trihydrosilanes pathway. Isotopic labeling experiments were also conducted to figure out the possible mechanism (see Supplemental Information for details).

The hydrosilylation reaction of alkynes and Ph_2SiH_2 catalyzed by $CoBr_2$•Xantphos is so fast that the rate-determining step (RDS) is less likely to be involved in this procedure. In order to simplify the complexity, we finally conducted quantitative kinetic studies of the reaction of **3a** with $PhSiH_3$ to determine the roles of **3a**, $PhSiH_3$, and catalyst at the RDS. Measurements of the initial rates (k_{in}) for the reaction of $PhSiH_3$ with different concentration of vinyl silane (**3a**) and catalyst showed a rise in the rates of the reactions. Plots of k_{in} versus the concentration of vinyl silane (Figures 1A and S2; Tables S2 and S3) and catalyst (Figures 1B and S4; Tables S6 and S7) gave two linear curves (slope = 1.59×10^{-4} Ms^{-1}; 4.35×10^{-2} Ms^{-1}), which suggested a first-order rate dependence on vinyl silane and catalyst (Figures 1A and 1B). Similar kinetic studies on $PhSiH_3$ showed no change in k_{in} (Figures 1C and S3; Tables S4 and S5), indicating a zero-order rate dependence on trihydrosilanes. These quantitative kinetic studies indicate that the vinyl silane coordination and insertion process is the RDS. Qualitative kinetic studies were also conducted. Measurement of reaction progress with different additives showed that $CoBr_2$•Xantphos had no effect on this transformation, and the reaction rates were slightly affected negatively by the

Please cite this article in press as: Guo et al., Cobalt-Catalyzed Asymmetric Synthesis of *gem*-Bis(silyl)alkanes by Double Hydrosilylation of Aliphatic Terminal Alkynes, Chem (2019), https://doi.org/10.1016/j.chempr.2019.02.001

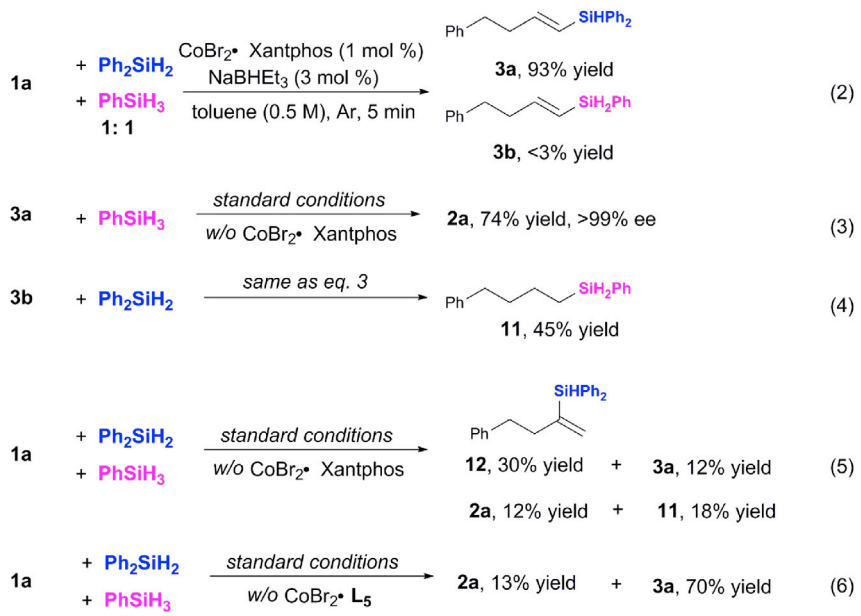

Scheme 6. Control Experiments

addition of 0.4 equiv of **2a** into the system, which indicated that there might be a competition between product and trihydrosilane to form the silyl cobalt species (Figures 1D and S1; Table S1).

According to the control experiments, deuterium experiments, qualitative and quantitative kinetic studies, and previous reports on cobalt-catalyzed hydrosilylation of unsaturated bond,[62,70–72] the most likely reaction mechanisms are proposed in Scheme 7. First, the precatalyst $CoBr_2$•Xantphos reacts with $NaBHEt_3$ to form cobalt hydride species **A**. Then alkyne undergoes coordination with species **A** followed by insertion into a Co–H bond to generate vinyl cobalt species **B**, which goes through σ-bond metathesis with Ph_2SiH_2 to afford vinyl silane **3** and regenerate cobalt hydride species **A**. Vinyl silane **3** can react with silyl cobalt species **C**, which is generated by the reaction of OIP•$CoBr_2$ with $PhSiH_3$ and $NaBHEt_3$, to deliver alkyl cobalt species **D**. The vinyl silane coordination and insertion process is the RDS. Species **D** goes through σ-bond metathesis with $PhSiH_3$ to reproduce species **C** and release product **2**.

The proposed mechanism is supported by DFT calculations. The free-energy changes of the most favorable pathway of Co-catalyzed sequential hydrosilylations of but-3-yn-1-ylbenzene are shown in Figure 2. The possible closed-shell singlet, open-shell singlet, and triplet-spin states were all explored, and the most stable singlet and triplet state energies are presented. The detailed energies of all spin states for each stationary point are included in Table S9. From the (Xantphos)CoH **cat1**, alkyne coordination leads to the (Xantphos)CoH(alkyne) species **int1**. Subsequent hydrometallation via **TS1** is facile and irreversible, generating the alkenylcobalt species **int2**. This alkenylcobalt species is not stable and undergoes facile σ-bond metathesis via **TS2** to produce the vinyl silane **3a** and regenerate the active (Xantphos)CoH catalyst. The vinyl silane **3a** coordinates to the (OIP)Co(SiH_2Ph) **cat2**, leading to **int4**. **int4** then undergoes the insertion of **3a** via **TS3**, and subsequent σ-bond metathesis of alkylcobalt species **int5** produces

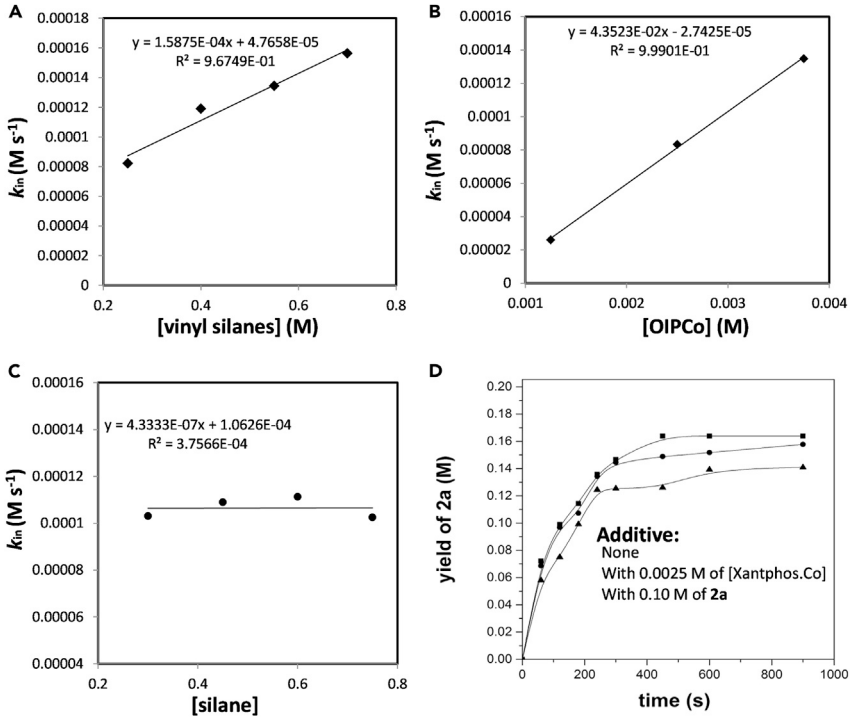

Figure 1. Qualitative and Quantitative Kinetic Studies
(A) A plot of k_{in} versus vinyl silane (**3a**) concentrations.
(B) A plot of k_{in} versus OIP.Co catalyst concentrations.
(C) A plot of kin versus phenyl silane concentrations.
(D) Time course study of **2a**.

the final disilylation product **2a** and regenerates **cat2**. According to the free-energy changes of the sequential catalytic cycles, the first hydrosilylation with (Xantphos) CoH is very efficient, and the hydrometalation step vis **TS1** determines the rate of the first hydrosilylation. The secondary hydrosilylation with (OIP)Co(SiH_2Ph) **cat2** has the alkene insertion via **TS3** and determines the overall rate, with a barrier of 20.1 kcal/mol from **int4** to **TS3**. Comparing the two catalytic cycles, the alkene insertion via **TS3** is the rate-limiting step of the dihydrosilylation, which is consistent with the above kinetic studies.

On the basis of the reaction mechanism, we next explored the regioselectivity of alkene insertion with the (OIP)Co(SiH_2Ph) catalyst. The competing regioisomeric insertions can occur via **TS3** or **TS5**, leading to the observed regioselectivity (Figure 3). **TS3** is 8.9 kcal/mol more favorable than **TS5** in terms of free energy, which is consistent with the experimental results showing that disilylation exclusively occurs at the same carbon center. The free-energy diagram of the corresponding catalytic cycle involving **TS5** is included in Figure S5. The origins of regioselectivity were further elucidated by distortion and interaction analysis.[73] The transition-state structure was separated into two distorted fragments, (OIP)Co(SiH_2Ph) and vinyl silane. $\Delta E_{dist\text{-}cat}$ refers to the energy penalty associated with the geometric change of the **cat2** fragment from the triplet **int4** to the corresponding geometry in **TS3** or **TS5**. $\Delta E_{dist\text{-}sub}$ refers to energy required for the geometric change of vinyl silane in the same process. The interaction energy ΔE_{int} reflects the stabilizing interaction between the two distorted fragments in the transition state. From the distortion and interaction analysis (Figure 3), we found that the interaction energy

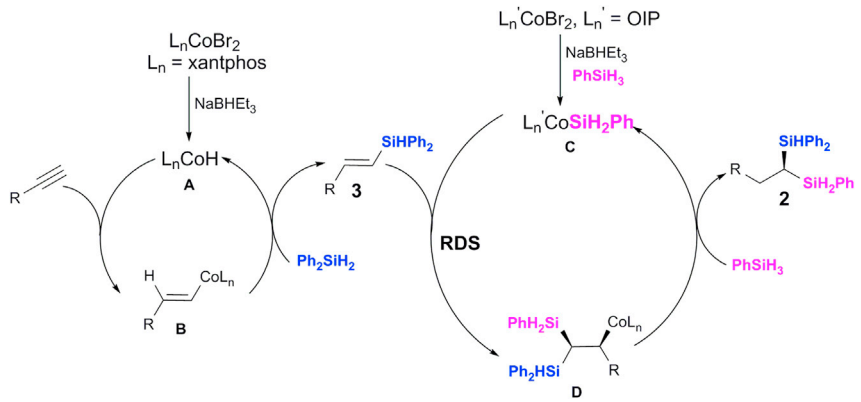

Scheme 7. The Proposed Mechanisms

is the leading contribution to the preference of **TS3**. The distortion energies are similar between the two transition states, suggesting that steric effects play a limited role in determining the regioselectivity. Therefore, the existing silyl group of vinyl silane directs the secondary silyl insertion and results in the exclusive disilylation at the same carbon center.

Conclusions

In summary, a cobalt-catalyzed sequential double hydrosilylation of aliphatic alkynes was developed to synthesize highly enantioenriched *gem*-bis(silyl)alkanes. To the best of our knowledge, this is the first time that this transformation has been achieved. The protocol used simple aliphatic alkynes and silanes, which were readily available from large-scale industrial processes or easily synthesized by a variety of efficient strategies, to construct the more valuable chiral *gem*-bis(silyl)alkanes. The synthetic versatility of *gem*-bis(silyl)alkanes was demonstrated by the synthesis of chiral organosilanols, α-hydroxysilanes, and hydrosilylation of alkynes to construct chiral silanes containing adjacent C- and Si-stereocenters. The control experiments, isotopic labeling experiments, and qualitative and quantitative kinetic studies were conducted to figure out the primary mechanism. DFT calculations were performed to elucidate the reaction mechanism and the origins of the regioselectivities. The primary mechanistic studies illustrated that the reaction might mainly undergo $CoBr_2$•Xantphos-catalyzed hydrosilylation of aliphatic alkynes with dihydrosilanes followed by OIP•$CoBr_2$-catalyzed asymmetric hydrosilylation of (*E*)-*β*-alkenyl silanes within the trihydrosilane pathway. Further studies will focus on exploring the potential utility of this unique chiral *gem*-bis(silyl)alkanes in materials science and pharmaceuticals.

EXPERIMENTAL PROCEDURES

Full experimental procedures are provided in the Supplemental Information.

Computational Details

All DFT calculations were performed with the Gaussian 09 program.[74] Geometry optimizations were carried out with the B3LYP[75–77]-D3 (Becke-Johnson damping function)[78,79] functional and def2-SVP basis sets[80] for all elements. The vibrational frequency was calculated at the same level of theory to identify each optimized stationary point as an energy minimum or a transition state and to evaluate the zero-point vibrational energy and thermal corrections at 298 K. On the basis of the gas-phase optimized structures, the single-point energies and solvent effects

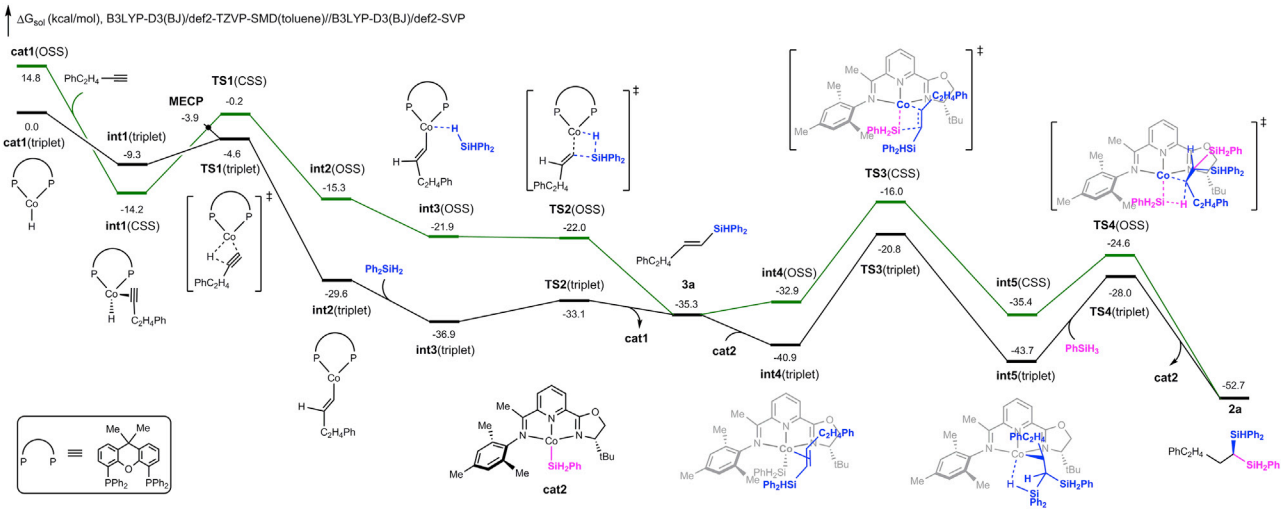

Figure 2. Free-Energy Diagram for the Most Favorable Reaction Pathways of Sequential Hydrosilylations of But-3-yn-1-ylbenzene
Spin states are shown in parentheses. OSS refers to open-shell singlet, and CSS refers to closed-shell singlet.

of toluene were calculated with the B3LYP-D3 functional and def2-TZVP basis sets[81] for all elements in the SMD solvent model.[82] The 3D diagrams of computed species were generated by CYLView.[83] Stability of wavefunction was confirmed for all organocobalt species.

Because the thermal corrections are based on the ideal gas model, this approach ignores the solvent suppression on the rotational and translational freedoms of solutes, resulting in overestimation of entropy contributions to the reaction free energies in solution.[84,85] To correct the entropy change in solution, we applied an empirical approach proposed by Martin and co-workers[86] because there is currently no widely accepted quantum-mechanics-based approach to correct entropy in solution. For each component change in a reaction at 298 K and 1 atm, a correction of 4.3 kcal/mol is applied to the reaction free energy (i.e., a reaction from m- to n-components has an additional free-energy correction for $(n - m) \times 4.3$ kcal/mol). This approach has been validated through a number of computational and experimental studies. Yu and co-workers have found that the entropy corrections are overestimated by about half in several cyclo-addition reactions.[87–89] Wang and co-workers have discovered the improved description of free-energy changes in a number of metal-catalyzed reactions by using the empirical approach from Martin.[90–93] In order to adjust the Gibbs free energies from 1 atm to 1 mol/L, a correction of RTln(cs/cg) (1.9 kcal/mol) is added to energies of all species. cs is the standard molar concentration in solution (1 mol/L), cg is the standard molar concentration in the gas phase (0.0446 mol/L), and R is the gas constant. Data from the zero-point correction (*ZPE*), thermal correction to enthalpy (*TCH*), thermal correction to Gibbs free energy (*TCG*), energies (*E*), enthalpies (*H*), and Gibbs free energies (*G*) (in Hartree) of the structures for all the figures calculated are shown in Table S8. Cartesian coordinates of the calculated species are shown in Table S10.

DATA AND SOFTWARE AVAILABILITY

The crystallography data have been deposited at the Cambridge Crystallographic Data Center (CCDC) under accession numbers CCDC: 1435434 (**L5**•$CoBr_2$) and

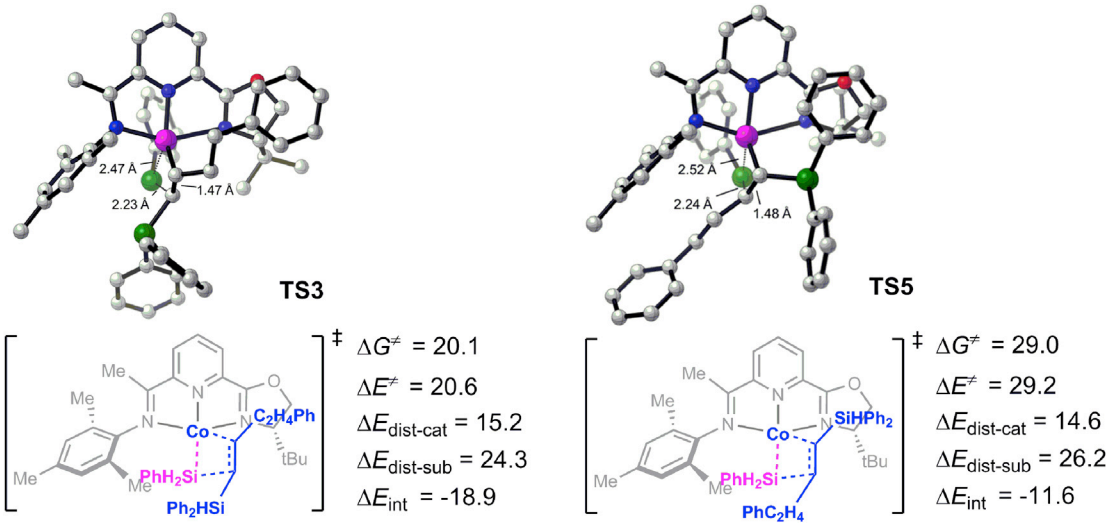

Figure 3. Optimized Structures, Energies, and Distortion and Interaction Analysis of the Regioisomeric Insertion Transition States with Vinyl Silane
Energy barriers in kcal/mol are compared to those of triplet **int4**. All hydrogens are omitted for clarity.

CCDC: 1845310 (**5e**) and can be obtained free of charge from http://www.ccdc.cam.ac.uk/getstructures.

SUPPLEMENTAL INFORMATION

Supplemental Information can be found with this article online at https://doi.org/10.1016/j.chempr.2019.02.001.

ACKNOWLEDGMENTS

We are grateful for financial support from National Natural Science Foundation of China (21772171 and 21472162 to Z.L.; 21702182 and 21873081 to X.H.), the Natural Science Foundation of Zhejiang Province (LR19B020001 to Z.L.), the National 973 Program (2015CB856600 to Z.L.), the Fundamental Research Funds for the Central Universities (2018QNA3009 to Z.L.), and Zhejiang University K.P. Chao's High Technology Development Foundation (to Z.L.) and the Chinese "Thousand Youth Talents Plan" (to X.H.). Calculations were performed on the high-performance computing system at the Zhejiang University Department of Chemistry. We thank Mr. Jiyong Liu at Zhejiang University for helping with X-ray diffraction analysis and reviewers for their constructive suggestions.

AUTHOR CONTRIBUTIONS

Conceptualization, Z.L. and J.G.; Methodology, Z.L., J.G., and H.W.; Investigation, J.G., H.W., and S.X.; Writing - original draft, J.G. and H.W.; Writing - review & editing, Z.L., X.H., J.G., and H.W.; Funding Acquisition, Z.L. and X.H.; Supervision, Z.L. and X.H.

DECLARATION OF INTERESTS

The authors declare no competing interests.

Received: August 22, 2018
Revised: November 18, 2018
Accepted: January 31, 2019
Published: February 28, 2019

REFERENCES AND NOTES

1. Hiyama, T., and Kusumoto, T. (1991). In Comprehensive Organic Synthesis, B.M. Trost and I. Fleming, eds. (Pergamon Press), pp. 763–792.
2. Masse, C.E., and Panek, J.S. (1995). Diastereoselective reactions of chiral allyl- and allenylsilanes with activated C=X π-bonds. Chem. Rev. *95*, 1293–1316.
3. Brook, M.A. (2000). Silicon in Organic, Organometallic and Polymer Chemistry (Wiley).
4. Brunner, H. (2004). A new hydrosilylation mechanism—new preparative opportunities. Angew. Chem. Int. Ed. *43*, 2749–2750.
5. Marciniec, B. (2009). Hydrosilylation: A Comprehensive Review on Recent Advances (Springer Science).
6. Zhang, H.J., Priebbenow, D.L., and Bolm, C. (2013). Acylsilanes: valuable organosilicon reagents in organic synthesis. Chem. Soc. Rev. *42*, 8540–8571.
7. Ojima, I. (1989). In The Chemistry of Organic Silicon Compounds, S. Patai and Z. Rappoport, eds. (Wiley).
8. Brook, M.A. (1999). In Silicon in Organic, Organometallic, and Polymer Chemistry, M.A. Brook, ed. (Wiley).
9. Ponomarenko, S.A., and Kirchmeyer, S. (2011). Conjugated organosilicon materials for organic electronics and photonics. Adv. Polym. Sci. *235*, 33–110.
10. Showell, G.A., and Mills, J.S. (2003). Chemistry challenges in lead optimization: Silicon isosteres in drug discovery. Drug Discov. Today *8*, 551–556.
11. Franz, A.K., and Wilson, S.O. (2013). Organosilicon molecules with medicinal applications. J. Med. Chem. *56*, 388–405.
12. Min, G.K., Hernández, D., and Skrydstrup, T. (2013). Efficient routes to carbon–silicon bond formation for the synthesis of silicon-containing peptides and azasilaheterocycles. Acc. Chem. Res. *46*, 457–470.
13. Gibson, S.E., and Rudd, M. (2007). The role of secondary interactions in the asymmetric palladium-catalysed hydrosilylation of olefins with monophosphane ligands. Adv. Synth. Catal. *349*, 781–795.
14. Uozumi, Y., and Hayashi, T. (1991). Catalytic asymmetric synthesis of optically active 2-alkanols via hydrosilylation of 1-alkenes with a chiral monophosphine-palladium catalyst. J. Am. Chem. Soc. *113*, 9888–9890.
15. Shimada, T., Mukaide, K., Shinohara, A., Han, J.W., and Hayashi, T. (2002). Asymmetric synthesis of 1-aryl-1,2-ethanediols from arylacetylenes by palladium-catalyzed asymmetric hydrosilylation as a key step. J. Am. Chem. Soc. *124*, 1584–1585.
16. Jensen, J.F., Svendsen, B.Y., la Cour, T.V., Pedersen, H.L., and Johannsen, M. (2002). Highly enantioselective hydrosilylation of aromatic alkenes. J. Am. Chem. Soc. *124*, 4558–4559.
17. Guo, X.-X., Xie, J.-H., Hou, G.-H., Shi, W.-J., Wang, L.-X., and Zhou, Q.-L. (2004). Asymmetric palladium-catalyzed hydrosilylation of styrenes using efficient chiral spiro phosphoramidite ligands. Tetrahedron Asymmetry *15*, 2231–2234.
18. Chen, J.-H., Cheng, B., Cao, M.-Y., and Lu, Z. (2015). Iron-catalyzed asymmetric hydrosilylation of 1,1-disubstituted alkenes. Angew. Chem. Int. Ed. *54*, 4661–4664.
19. Gribble, M.W., Jr., Pirnot, M.T., Bandar, J.S., Liu, R.Y., and Buchwald, S.L. (2017). Asymmetric copper hydride-catalyzed Markovnikov hydrosilylation of vinylarenes and vinyl heterocycles. J. Am. Chem. Soc. *139*, 2192–2195.
20. Cheng, B., Lu, P., Zhang, H., Cheng, X., and Lu, Z. (2017). Highly enantioselective cobalt-catalyzed hydrosilylation of alkenes. J. Am. Chem. Soc. *139*, 9439–9442.
21. Cheng, B., Liu, W., and Lu, Z. (2018). Iron-catalyzed highly enantioselective hydrosilylation of unactivated terminal alkenes. J. Am. Chem. Soc. *140*, 5014–5017.
22. Guo, J., Shen, X., and Lu, Z. (2017). Regio- and enantioselective cobalt-catalyzed sequential hydrosilylation/hydrogenation of terminal alkynes. Angew. Chem. Int. Ed. *56*, 615–618.
23. Igawa, K., Yoshihiro, D., Ichikawa, N., Kokan, N., and Tomooka, K. (2012). Catalytic enantioselective synthesis of alkenylhydrosilanes. Angew. Chem. Int. Ed. *51*, 12745–12748.
24. Wen, H., Wan, X., and Huang, Z. (2018). Asymmetric synthesis of silicon-stereogenic vinylhydrosilanes via cobalt-catalyzed regio- and enantioselective alkyne hydrosilylation with dihydrosilanes. Angew. Chem. Int. Ed. *57*, 6319–6323.
25. Shintani, R. (2015). Recent advances in the transition-metal-catalyzed enantioselective synthesis of silicon-stereogenic organosilanes. Asian J. Org. Chem. *4*, 510–514.
26. Bauer, J.O., and Strohmann, C. (2016). Recent progress in asymmetric synthesis and application of difunctionalized silicon-stereogenic silanes. Eur. J. Inorg. Chem. *2016*, 2868–2881.
27. Hayashi, T., Yamamoto, K., and Kumada, M. (1974). Asymmetric synthesis of bifunctional organosilicon compounds via hydrosilylation. Tetrahedron Lett. *15*, 331–334.
28. Schmidt, D.R., O'Malley, S.J., and Leighton, J.L. (2003). Catalytic asymmetric silane alcoholysis: practical access to chiral silanes. J. Am. Chem. Soc. *125*, 1190–1191.
29. Yasutomi, Y., Suematsu, H., and Katsuki, T. (2010). Iridium(III)-catalyzed enantioselective Si-H bond insertion and formation of an enantioenriched silicon center. J. Am. Chem. Soc. *132*, 4510–4511.
30. Shintani, R., Moriya, K., and Hayashi, T. (2011). Palladium-catalyzed enantioselective desymmetrization of silacyclobutanes: construction of silacycles possessing a tetraorganosilicon stereocenter. J. Am. Chem. Soc. *133*, 16440–16443.
31. Shintani, R., Otomo, H., Ota, K., and Hayashi, T. (2012). Palladium-catalyzed asymmetric synthesis of silicon-stereogenic dibenzosiloles via enantioselective C–H bond functionalization. J. Am. Chem. Soc. *134*, 7305–7308.
32. Zhang, Y.Z., Zhu, S.F., Wang, L.X., and Zhou, Q.L. (2008). Copper-catalyzed highly enantioselective carbenoid insertion into Si-H bonds. Angew. Chem. Int. Ed. *47*, 8496–8498.
33. Chen, D., Zhu, D.X., and Xu, M.H. (2016). Rhodium(I)-catalyzed highly enantioselective insertion of carbenoid into Si–H: efficient access to functional chiral silanes. J. Am. Chem. Soc. *138*, 1498–1501.
34. Kan, S.B.J., Lewis, R.D., Chen, K., and Arnold, F.H. (2016). Directed evolution of cytochrome c for carbon–silicon bond formation: bringing silicon to life. Science *354*, 1048–1051.
35. Gao, L., Zhang, Y.-B., and Song, Z.-L. (2013). Exploration of versatile geminal bis(silane) chemistry. Synlett *24*, 139–144.
36. Inoue, A., Kondo, J., Shinokubo, H., and Oshima, K. (2002). Facile synthesis of ketones from 1,1-disilylethenes via oxidation of gem-disilylalkanes. Chem. Commun. 114–115.
37. Liu, Z.-J., Lin, X.-L., Yang, N., Su, Z.-S., Hu, C.-W., Xiao, P.-H., He, Y.-Y., and Song, Z.-L. (2016). Unique steric effect of geminal bis(silane) to control the high exo-selectivity in intermolecular Diels–Alder reaction. J. Am. Chem. Soc. *138*, 1877–1883.
38. Zhang, Y.-B., Guo, Q.-Y., Sun, X.-W., Lu, J., Cao, Y.-J., Pu, Q., Chu, Z.-W., Gao, L., and Song, Z.-L. (2018). Total synthesis of bryostatin 8 using an organosilane-based strategy. Angew. Chem. Int. Ed. *57*, 942–946.
39. Cahiez, G., and Moyeux, A. (2010). Cobalt-catalyzed cross-coupling reactions. Chem. Rev. *110*, 1435–1462.
40. Gao, K., and Yoshikai, N. (2014). Low-valent cobalt catalysis: new opportunities for C–H functionalization. Acc. Chem. Res. *47*, 1208–1219.
41. Pellissier, H., and Clavier, H. (2014). Enantioselective cobalt-catalyzed transformations. Chem. Rev. *114*, 2775–2823.
42. Moselage, M., Li, J., and Ackermann, L. (2016). Cobalt-catalyzed C–H activation. ACS Catal. *6*, 498–525.
43. Pellissier, H. (2018). Recent developments in enantioselective cobalt-catalyzed transformations. Coord. Chem. Rev. *360*, 122–168.
44. Friedfeld, M.R., Shevlin, M., Hoyt, J.M., Krska, S.W., Tudge, M.T., and Chirik, P.J. (2013). Cobalt precursors for high-throughput discovery of base metal asymmetric alkene hydrogenation catalysts. Science *342*, 1076–1080.
45. Zhang, L., Zuo, Z.-Q., Wan, X.-L., and Huang, Z. (2014). Cobalt-catalyzed enantioselective hydroboration of 1,1-disubstituted aryl

alkenes. J. Am. Chem. Soc. *136*, 15501–15504.

46. Chen, J.-H., Xi, T., Ren, X., Cheng, B., Guo, J., and Lu, Z. (2014). Asymmetric cobalt catalysts for hydroboration of 1,1-disubstituted alkenes. Org. Chem. Front. *1*, 1306–1309.

47. Friedfeld, M.R., Shevlin, M., Margulieux, G.W., Campeau, L.C., and Chirik, P.J. (2016). Cobalt-catalyzed enantioselective hydrogenation of minimally functionalized alkenes: isotopic labeling provides insight into the origin of stereoselectivity and alkene insertion preferences. J. Am. Chem. Soc. *138*, 3314–3324.

48. Huang, Y., Huang, R.Z., and Zhao, Y. (2016). Cobalt-catalyzed enantioselective vinylation of activated ketones and imines. J. Am. Chem. Soc. *138*, 6571–6576.

49. Yang, J.-F., Rérat, A., Lim, Y.J., Gosmini, C., and Yoshikai, N. (2017). Cobalt-catalyzed enantio- and diastereoselective intramolecular hydroacylation of trisubstituted alkenes. Angew. Chem. Int. Ed. *56*, 2449–2453.

50. Yu, S.-J., Wu, C.-Z., and Ge, S.-Z. (2017). Cobalt-catalyzed asymmetric hydroboration/cyclization of 1,6-enynes with pinacolborane. J. Am. Chem. Soc. *139*, 6526–6529.

51. Jiang, H.-L., Lang, K., Lu, H.-J., Wojtas, L., and Zhang, X.P. (2017). Asymmetric radical bicyclization of allyl azidoformates via cobalt(II)-based metalloradical catalysis. J. Am. Chem. Soc. *139*, 9164–9167.

52. Kim, D.K., Riedel, J., Kim, R.S., and Dong, V.M. (2017). Cobalt catalysis for enantioselective cyclobutanone construction. J. Am. Chem. Soc. *139*, 10208–10211.

53. Guo, J., Cheng, B., Shen, X.-Z., and Lu, Z. (2017). Cobalt-catalyzed asymmetric sequential hydroboration/hydrogenation of internal alkynes. J. Am. Chem. Soc. *139*, 15316–15319.

54. Friedfeld, M.R., Zhong, H.-Y., Ruck, R.T., Shevlin, M., and Chirik, P.J. (2018). Cobalt-catalyzed asymmetric hydrogenation of enamides enabled by single-electron reduction. Science *360*, 888–893.

55. Pagar, V.V., and RajanBabu, T.V. (2018). Tandem catalysis for asymmetric coupling of ethylene and enynes to functionalized cyclobutanes. Science *361*, 68–72.

56. Wu, C.-Z., Teo, W.J., and Ge, S.-Z. (2018). Cobalt-catalyzed (*e*)-selective anti-Markovnikov hydrosilylation of terminal alkynes. ACS Catal. *8*, 5896–5900.

57. Sahar, Bari, A., Irfan, M., Zara, Z., Eliasson, B., Ayub, K., and Iqbal, J. (2017). Benchmark study of bond dissociation energy of SieX (X=F, Cl, Br, N, O, H and C) bond using density functional theory (DFT). J. Mol. Struct. *1143*, 8–19.

58. Lee, K.L. (2017). (Aminomethyl)pyridine complexes for the cobalt-catalyzed anti-Markovnikov hydrosilylation of alkoxy- or siloxy(vinyl)silanes with alkoxy- or siloxyhydrosilanes. Angew. Chem. Int. Ed. *56*, 3665–3669.

59. Gao, Y., Wang, L., and Deng, L. (2018). Distinct catalytic performance of cobalt(I) *N*-heterocyclic carbene complexes in promoting the reaction of alkene with diphenylsilane: selective 2,1-hydrosilylation, 1,2-hydrosilylation, and hydrogenation of alkene. ACS Catal. *8*, 9637–9646.

60. Chandrasekhar, V., Boomishankar, R., and Nagendran, S. (2004). Recent developments in the synthesis and structure of organosilanols. Chem. Rev. *104*, 5847–5910.

61. Visco, M.D., Wieting, J.M., and Mattson, A.E. (2016). Carbon–silicon bond formation in the synthesis of benzylic Silanes. Org. Lett. *18*, 2883–2885.

62. Wang, C., Teo, W.J., and Ge, S.-Z. (2017). Cobalt-catalyzed regiodivergent hydrosilylation of vinylarenes and aliphatic alkenes: ligand- and silane-dependent regioselectivities. ACS Catal. *7*, 855–863.

63. Trost, B.M., and Ball, Z.T. (2001). Markovnikov alkyne hydrosilylation catalyzed by ruthenium complexes. J. Am. Chem. Soc. *123*, 12726–12727.

64. Hirone, N., Sanjiki, H., Tanaka, R., Hata, T., and Urabe, H. (2010). Acceleration of the substitution of silanes with Grignard reagents by using either LiCl or YCl_3/MeLi. Angew. Chem. Int. Ed. *49*, 7762–7764.

65. Shin, K., Joung, S., Kim, Y., and Chang, S. (2017). Selective synthesis of silacycles by borane-catalyzed domino hydrosilylation of proximal unsaturated bonds: tunable approach to 1,n-diols. Adv. Synth. Catal. *359*, 3428–3436.

66. Fleming, I., Barbero, A., and Walter, D. (1997). Stereochemical control in organic synthesis using silicon-containing compounds. Chem. Rev. *97*, 2063–2192.

67. Zhan, G., Teng, H.L., Luo, Y., Lou, S.J., Nishiura, M., and Hou, Z. (2018). Enantioselective construction of silicon-stereogenic silanes by scandium-catalyzed intermolecular alkene hydrosilylation. Angew. Chem. Int. Ed. *57*, 12342–12346.

68. Xu, L.W., Li, L., Lai, G.Q., and Jiang, J.X. (2011). The recent synthesis and application of silicon-stereogenic silanes: a renewed and significant challenge in asymmetric synthesis. Chem. Soc. Rev. *40*, 1777–1790.

69. Mo, Z., Xiao, J., Gao, Y., and Deng, L. (2014). Regio- and stereoselective hydrosilylation of alkynes catalyzed by three-coordinate cobalt(I) alkyl and silyl complexes. J. Am. Chem. Soc. *136*, 17414–17417.

70. Ciancanelli, R., Noll, B.C., DuBois, D.L., and DuBois, M.R. (2002). Comprehensive thermodynamic characterization of the metal-hydrogen bond in a series of cobalt-hydride complexes. J. Am. Chem. Soc. *124*, 2984–2992.

71. Sun, J., and Deng, L. (2016). Cobalt complex-catalyzed hydrosilylation of alkenes and alkynes. ACS Catal. *6*, 290–300.

72. Liu, Y., and Deng, L. (2017). Mode of activation of cobalt(II) amides for catalytic hydrosilylation of alkenes with tertiary silanes. J. Am. Chem. Soc. *139*, 1798–1801.

73. Bickelhaupt, F.M., and Houk, K.N. (2017). Analyzing reaction rates with the distortion/interaction-activation strain model. Angew. Chem. Int. Ed. *56*, 10070–10086.

74. Frisch, M.J., Trucks, G.W., Schlegel, H.B., Scuseria, G.E., Robb, M.A., Cheeseman, J.R., Scalmani, G., Barone, V., Mennucci, B., Petersson, G.A., et al. (2010). Gaussian 09, Revision C.01 (Gaussian Inc).

75. Lee, C., Yang, W., and Parr, R.G. (1988). Development of the Colle-Salvetti correlation-energy formula into a functional of the electron density. Phys. Rev., B Condens. Matter. *37*, 785–789.

76. Becke, A.D. (1993). Density-functional thermochemistry. III. The role of exact exchange. J. Chem. Phys. *98*, 5648–5652.

77. Stephens, P.J., Devlin, F.J., Chabalowski, C.F., and Frisch, M.J. (1994). Ab initio calculation of vibrational absorption and circular dichroism spectra using density functional force fields. J. Phys. Chem. *98*, 11623–11627.

78. Grimme, S., Antony, J., Ehrlich, S., and Krieg, H. (2010). A consistent and accurate *ab initio* parametrization of density functional dispersion correction (DFT-D) for the 94 elements H-Pu. J. Chim. Phys. *132*, 154104.

79. Grimme, S., Ehrlich, S., and Goerigk, L. (2011). Effect of the damping function in dispersion corrected density functional theory. J. Comput. Chem. *32*, 1456–1465.

80. Schäfer, A., Horn, H., and Ahlrichs, R. (1992). Fully optimized contracted Gaussian basis sets for atoms Li to Kr. J. Chem. Phys. *97*, 2571–2577.

81. Weigend, F., and Ahlrichs, R. (2005). Balanced basis sets of split valence, triple zeta valence and quadruple zeta valence quality for H to Rn: design and assessment of accuracy. Phys. Chem. Chem. Phys. *7*, 3297–3305.

82. Marenich, A.V., Cramer, C.J., and Truhlar, D.G. (2009). Universal solvation model based on solute electron density and on a continuum model of the solvent defined by the bulk dielectric constant and atomic surface tensions. J. Phys. Chem. B *113*, 6378–6396.

83. Legault, C.Y. (2009). CYLview, 1.0b (Université de Sherbrooke). http://www.cylview.org.

84. Wertz, D.H. (1980). Relationship between the gas-phase entropies of molecules and their entropies of solvation in water and 1-octanol. J. Am. Chem. Soc. *102*, 5316–5322.

85. Leung, B.O., Reid, D.L., Armstrong, D.A., and Rauk, A. (2004). Entropies in solution from entropies in the gas phase. J. Phys. Chem. A *108*, 2720–2725.

86. Martin, R.L., Hay, P.J., and Pratt, L.R. (1998). Hydrolysis of ferric ion in water and

conformational equilibrium. J. Phys. Chem. A *102*, 3565–3573.

87. Yu, Z.X., and Houk, K.N. (2003). Intramolecular 1,3-dipolar ene reactions of nitrile oxides occur by stepwise 1,1-cycloaddition/retro-ene mechanisms. J. Am. Chem. Soc. *125*, 13825–13830.

88. Chen, Y., Ye, S., Jiao, L., Liang, Y., Sinha-Mahapatra, D.K., Herndon, J.W., and Yu, Z.X. (2007). Mechanistic Twist of the [8+2] cycloadditions of dienylisobenzofurans and dimethyl acetylenedicarboxylate: stepwise [8+2] versus [4+2]/[1,5]-vinyl shift mechanisms revealed through a theoretical and experimental study. J. Am. Chem. Soc. *129*, 10773–10784.

89. Liang, Y., Liu, S., Xia, Y., Li, Y., and Yu, Z.X. (2008). Mechanism, regioselectivity, and the kinetics of phosphine-catalyzed [3+2] cycloaddition reactions of allenoates and electron-deficient alkenes. Chemistry *14*, 4361–4373.

90. Li, H., Jiang, J., Lu, G., Huang, F., and Wang, Z.-X. (2011). On the "reverse gear" mechanism of the reversible dehydrogenation/hydrogenation of a nitrogen heterocycle catalyzed by a Cp*Ir complex: a computational study. Organometallics *30*, 3131–3141.

91. Li, H., Wen, M., and Wang, Z.X. (2012). Computational mechanistic study of the hydrogenation of carbonate to methanol catalyzed by the Ru(II)PNN complex. Inorg. Chem. *51*, 5716–5727.

92. Wen, M., Huang, F., Lu, G., and Wang, Z.X. (2013). Density functional theory mechanistic study of the reduction of CO_2 to CH_4 catalyzed by an ammonium hydridoborate ion pair: CO_2 activation via formation of a formic acid entity. Inorg. Chem. *52*, 12098–12107.

93. Qu, S., Dang, Y., Song, C., Wen, M., Huang, K.W., and Wang, Z.X. (2014). Catalytic mechanisms of direct pyrrole synthesis via dehydrogenative coupling mediated by PNP-Ir or PNN-Ru pincer complexes: crucial role of proton-transfer shuttles in the PNP-Ir system. J. Am. Chem. Soc. *136*, 4974–4991.